frontiers in Energy Research

ORIGINAL RESEARCH
published: 07 May 2021
doi: 10.3389/fenrg.2021.680761

Pore Structure Regulation and Electrochemical Performance Characterization of Activated Carbon for Supercapacitors

Shijie Li[1,2], Tao Xing[2], Yilin Wang[1], Pengwei Lu[1], Weixue Kong[1], Shenao Li[1], Xiaomin Su[1] and Xinkuan Wei[1]*

[1] School of Thermal Engineering, Shandong Jianzhu University, Jinan, China, [2] Shandong Energy Group Co., Ltd. Jinan, China

In order to achieve the purpose of regulating the pore structure characteristics of activated carbon by adjusting the experimental parameters, the effects of carbonization temperature, carbonization time, pre-activation temperature, pre-activation time and impregnation time on the pore structure of sargassum-based activated carbon (SAC) are studied by orthogonal experiment. The gravimetric capacitance of SAC and the relationship between the gravimetric capacitance and specific surface area are also studied. The results show that the SACs prepared at all experimental conditions have developed pore structure and huge specific surface area, reaching 3,122 m^2/g. The pore size of SAC is almost all within 6 nm, in which the micropores are mainly concentrated in 0.4–0.8 nm, the mesopores are mainly concentrated in 2–4 nm, and the number of micropores is significantly higher than that of mesopores. During the preparation of SAC, the effect of carbonization temperature on the specific surface area and specific pore volume of SAC is very significant. The effect of carbonization time on the specific surface area of SAC is significant, but the effect on specific pore volume can be ignored. The effects of pre-activation temperature, pre-activation time, and impregnation time on specific surface area and specific pore volume of SAC can be ignored. In addition, SACs show good gravimetric capacitance performance as electrode material for supercapacitors, which can significantly increase the capacitance of supercapacitors and thus broaden their applications. The gravimetric capacitance and specific surface area of SACs show a good linear relationship when the activated carbons have similar material properties and pore size distribution.

Keywords: activated carbon, pore structure, regulation, specific surface area, gravimetric capacitance

OPEN ACCESS

Edited by:
Dong Wang,
Columbia University, United States

Reviewed by:
Xiaotong Ma,
Shandong University of Science and Technology, China
Yin Qian,
National University of Defense Technology, China

****Correspondence:***
Shijie Li
675767978@163.com

Specialty section:
This article was submitted to Bioenergy and Biofuels, a section of the journal Frontiers in Energy Research

Received: *15 March 2021*
Accepted: *12 April 2021*
Published: *07 May 2021*

Citation:
Li S, Xing T, Wang Y, Lu P, Kong W, Li S, Su X and Wei X (2021) Pore Structure Regulation and Electrochemical Performance Characterization of Activated Carbon for Supercapacitors. Front. Energy Res. 9:680761. doi: 10.3389/fenrg.2021.680761

INTRODUCTION

High energy costs, continuous consumption of fossil fuels and climate change caused by greenhouse gas emissions have led to a shift in energy demand to renewable and clean energy (Abioye and Ani, 2015; Deng et al., 2016; Qiu et al., 2018; Guo et al., 2019). Therefore, the development of clean energy such as solar energy, wind energy and ocean energy has increased, but these renewable

energy resources are intermittent and unstable. In order to make full use of the electric energy generated by these renewable clean energy, an effective energy storage system must be established (Pintor et al., 2013). At present, traditional capacitors and batteries are the two most commonly used energy storage devices, but they have their own disadvantages. The traditional capacitor can discharge in a few seconds with high power density, but its energy density is not ideal because of its electrostatic energy storage mode. Battery has high energy density due to its chemical energy storage mode, but its discharge speed is slow and power density is not ideal (Simon and Gogotsi, 2008; Farma et al., 2013; Wang et al., 2015). Supercapacitor with electrochemical performance between traditional capacitor and battery is considered to be a promising energy storage device (Guo et al., 2018a,b; Wang J.-G. et al., 2018; Hou et al., 2019). It has the characteristics of high power density, long cycle life, stable operation, fast charge and discharge time, appropriate size and weight, low cost and environmental friendliness (Chen et al., 2017; Lee et al., 2017; Miller et al., 2018; Shao et al., 2018; Li et al., 2019; Liu et al., 2019; Zhang et al., 2019). However, the electrochemical performance of supercapacitors is limited by their electrode materials. Therefore, in order to meet the application of higher energy storage requirements, such as portable electronic products, hybrid electric vehicles and large-scale industrial equipment, it is necessary to develop new electrode materials or improve the characteristics of electrode materials to greatly improve the performance of supercapacitors (Xiao et al., 2014).

Electrode material is the most important factor to determine the electrochemical performance of supercapacitors. Carbon materials are the most widely used electrode materials for supercapacitors. At present, more than 80% of commercial supercapacitors in the world are assembled based on carbon materials (Shao et al., 2017; Cao H. et al., 2018; Cao Y. et al., 2018; Saeed et al., 2018; Tseng et al., 2018; Wang D. et al., 2018). Carbon materials are considered to be the most promising electrode materials for supercapacitors in the future due to their low cost, various existing forms, huge specific surface area, good conductivity, good physical and chemical stability in different electrolytes (from strong acid to alkaline). Among them, activated carbon has become the most widely used electrode materials for supercapacitors due to its abundant raw materials, mature preparation method and non-toxicity (Zhang et al., 2018; Wang et al., 2019). Generally, carbon electrode materials require highly developed pore structure, appropriate pore size distribution and surface characteristics to exhibit excellent electrochemical performance (Wang and Kaskel, 2012; Hao et al., 2013; Liu et al., 2013; Zhang et al., 2013). Therefore, adjusting the pore structure and surface chemistry of porous carbon is the key to optimize capacitor electrode materials. At present, activated carbon prepared by different activation methods from different precursors (such as wood, coal, and fruit shell) is the most commonly used electrode material (White et al., 2009; Titirici and Antonietti, 2010). There are many studies about adopting biomass for activated carbons preparation, but the usage of algae is rarely included. Yu et al. (2015), who prepared the mesophase carbon particles from gulfweed by H_2SO_4 hydrothermal method, and finally a kind of activated carbon with strong adsorption capacity of fluoride was prepared. Gulfweed-based activated carbons also have been made for the destination to support selective catalytic, which was prepared by both physical activation and co-activation (Li et al., 2015). The specific surface area of many activated carbons is not large enough and the pore size distribution is too wide, which is not conducive to the improvement of capacitance. In order to improve the capacitance performance of supercapacitor and accelerate its application, the research of activated carbon needs innovation urgently. The innovative research of activated carbon electrode materials is mainly carried out in two aspects. The first is to explore new precursors and activation technology, which will open up a new way to prepare new activated carbon electrode materials with huge specific surface area and reasonable pore size distribution. Another is to explore the effective pore structure regulation technology of activated carbon to improve the surface area utilization of activated carbon electrode materials, so as to improve the capacity and stability of the supercapacitor. In this study, the effective regulation technology of pore structure of activated carbon was researched by studying the influence of experimental factors on the pore structure characteristics. In addition, the electrochemical properties of the prepared activated carbon for supercapacitors and the relationship between the electrochemical properties and specific surface area were also studied.

EXPERIMENTAL

Materials

Sargassum used in this experiment was collected from Rongcheng Maoquan Aquatic Products Co., Ltd., in Shandong Province, China. And the products of the company were mainly derived from Yellow Sea. Ultimate and proximate analyses of the sargassum are shown in **Table 1**. The collected sargassum was washed thoroughly and dried in a blast drying oven for 48 h at a drying temperature of 120°C. After sufficient drying, the sargassum was crushed and sieved with a quick grinder and a vibrating screen, respectively, and the products with particle size less than 180 μm were obtained for standby.

Methods

The preparation of activated carbon usually requires several processes, including carbonization, low temperature pre-activation, and high temperature activation. The flow chart of the experiment procedures is shown in **Figure 1**. The effects of carbonization and pre-activation conditions on the pore structure characteristics of activated carbon were studied.

TABLE 1 | Ultimate and proximate analyses of the sargassum.

Ultimate analysis (wt%) (ad)					Proximate analysis (wt%) (ad)			
C	H	O	N	S	M	A	FC	V
41.41	5.42	34.98	3.39	1.67	2.40	10.73	14.93	71.94

M, moisture; A, ash; FC, fixed carbon; V, volatile.

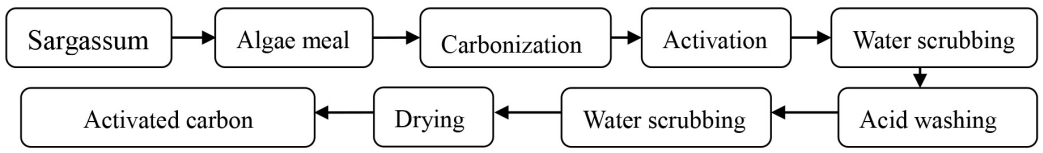

FIGURE 1 | The flow chart of the experiment procedures.

L_{16} (4^5) orthogonal experiment table without interaction was adopted to arrange the experiment. The factors and levels of orthogonal experiment are shown in **Table 2**.

Sargassum was carbonized in nitrogen atmosphere. The carbonization temperature was T_C, the carbonization time was t_C, the heating rate was 5°C/min, and the nitrogen flow rate was 2 L/min. The carbon products obtained from carbonization were put into nickel crucible, fully mixed with KOH solution in an impregnation ratio of 4:1 and then put into a drying oven for a certain time (t_I) at 80°C. Then the mixture was put into an atmosphere muff furnace for activation. In the activation process, the pre-activation temperature was T_P, the pre-activation time was t_P, the activation temperature was 800°C, the activation time was 120 min, and the heating rate was always 5°C/min. After activation, the nickel crucible was taken out and naturally cooled to ambient temperature. The obtained products were washed with deionized water at 80°C, then pickled to neutral with 0.1 mol/L hydrochloric acid solution, and finally washed with deionized water at 80°C. The obtained carbon products were put into a drying oven and dried at 120°C for 24 h.

Preparation of Supercapacitor

The activated carbon, conductive graphite and binder (PTFE emulsion) were mixed according to the mass ratio of 8:1:1, an appropriate amount of anhydrous ethanol was added to obtain the slurry, and the ultrasonic treatment was carried out for 30 min by ultrasonic cell breakers. The mixture was fully mixed, then the slurry was put into the air drying oven, and the excess ethanol was evaporated at 80°C, until the solution became thicker slurry. The slurry was evenly coated to the round nickel foam with a diameter of 1.5 cm, and the active material mass was about 5 mg. Put the coated nickel foam in the vacuum drying oven for 12 h at 120°C to evaporate the excess anhydrous ethanol in the electrode. The dried electrodes were put into a hydraulic press and pressed for 1 min under 14 MPa pressure. The electrodes and the diaphragm were assembled into a supercapacitor in the order of electrodes, diaphragms and electrodes, with an electrolyte of 6 mol/L potassium hydroxide solution.

TABLE 2 | Factors and levels of orthogonal experiment.

Level	Factor				
	T_C A (°C)	t_C B (min)	T_P C (°C)	t_P D (min)	t_I E (h)
Level 1	600	120	300	30	2
Level 2	650	180	350	45	4
Level 3	700	240	400	60	6
Level 4	750	300	450	75	8

T_C, carbonization temperature; t_C, carbonization time; T_P, pre-activation temperature; t_P, pre-activation time; t_I, impregnation time.

Experimental Techniques

Nitrogen (N_2) adsorption–desorption measurements were carried out at 77 K by employing an JW-BK132F (JWGB Sci & Tech Ltd.). Based on N_2 adsorption–desorption isotherms, the specific surface area of activated carbons was calculated by using BET method, isotherms were employed to calculate the specific surface area at a relative pressure range of 0.05–0.3. Combined with the adsorption isotherm data, the pore size distribution of mesopores and micropores was determined by BJH and HK method, respectively. To investigate the electrochemical properties of activated carbons, the cyclic voltammetry (CV) and galvanostatic charge–discharge (GCD) test were measured on an electrochemical station (CHI760E, CH Instruments).

RESULTS AND DISCUSSION

Sixteen groups of activated carbon samples were prepared from sargassum according to the L_{16} (4^5) orthogonal experiment, and the pore structure characteristics of activated carbons were characterized. The results are shown in **Table 3**.

TABLE 3 | Experiment and results of orthogonal design.

Number	T_C A (°C)	t_C B (min)	T_P C (°C)	t_P D (min)	t_I E (h)	S_{BET} (m^2/g)	V (cm^3/g)
1	600	120	300	30	2	2,955.9	2.50
2	600	180	350	45	4	3,110.8	2.74
3	600	240	400	60	6	3,122.0	2.56
4	600	300	450	75	8	1,861.5	1.59
5	650	120	350	60	8	2,676.0	1.56
6	650	180	300	75	6	2,550.3	1.47
7	650	240	450	30	4	2,379.4	1.27
8	650	300	400	45	2	2,756.6	1.50
9	700	120	400	75	4	2,313.1	0.92
10	700	180	450	60	2	2,393.3	1.19
11	700	240	300	45	8	2,588.8	0.89
12	700	300	350	30	6	1,716.1	0.83
13	750	120	450	45	6	1,881.9	0.84
14	750	180	400	30	8	1,923.0	0.87
15	750	240	350	75	2	1,790.2	0.76
16	750	300	300	60	4	1,484.9	0.57

S_{BET}, specific surface area; V, specific pore volume.

TABLE 4 | The range analysis of specific surface area.

	T_C A (°C)	t_C B (min)	T_P C (°C)	t_P D (min)	t_I E (h)	S_{BET} (m^2/g)
K_1	11,050.2	9,826.9	9,579.9	8,974.4	9,896.0	
K_2	10,362.3	9,977.4	9,293.1	10,338.1	9,288.2	
K_3	9,011.3	9,880.4	10,114.7	9,676.2	9,270.3	
K_4	7,080.0	7,819.1	8,516.1	8,515.1	9,049.3	Σ = 37503.8
k_1	2,762.6	2,456.7	2,395.0	2,243.6	2,474.0	Σ/16 = 2344.0
k_2	2,590.6	2,494.4	2,323.3	2,584.5	2,322.1	
k_3	2,252.8	2,470.1	2,528.7	2,419.1	2,317.6	
k_4	1,770.0	1,954.8	2,129.0	2,128.8	2,262.3	
R	992.6	539.6	399.7	455.7	212.0	

TABLE 5 | The variance analysis of specific surface area.

SV	SS	df	MS	F	Effect
A	2,295,088.9	3	765,029.6	30.9	Very significant
B	810,837.4	3	270,279.1	10.9	Significant
C	333,388.3	3	111,129.4	4.5	Not significant
D	479,547.0	3	159,849.0	6.5	Not significant
Error	99,003.6	4	24,750.88813		

$F_{0.01}(3, 4) = 16.69$; $F_{0.05}(3, 4) = 6.59$.
SV, source of variation; SS, sum of square; df, degree of freedom; MS, mean square.

The prepared activated carbons were marked as AC_1–AC_{16} according to the serial number. As can be seen from **Table 3** that all SACs have a large specific surface area (≥1,484.9 m^2/g), of which the maximum specific surface area is 3,122 m^2/g and the maximum specific pore volume is 2.74 cm^3/g, indicating that SAC has good application potential in adsorption, gas storage and supercapacitor carbon electrode materials.

Effect of Experimental Factors on Specific Surface Area of SAC

Range Analysis of Specific Surface Area

The range analysis of specific surface area is shown in **Table 4**. K_i (i = 1, 2, 3, 4) is the sum of the specific surface area value at a certain level in **Table 3**, k_i is the average value of K_i, and R is the range. It can be seen from **Table 4** that the range of specific surface area is $R_A > R_B > R_D > R_C > R_E$,

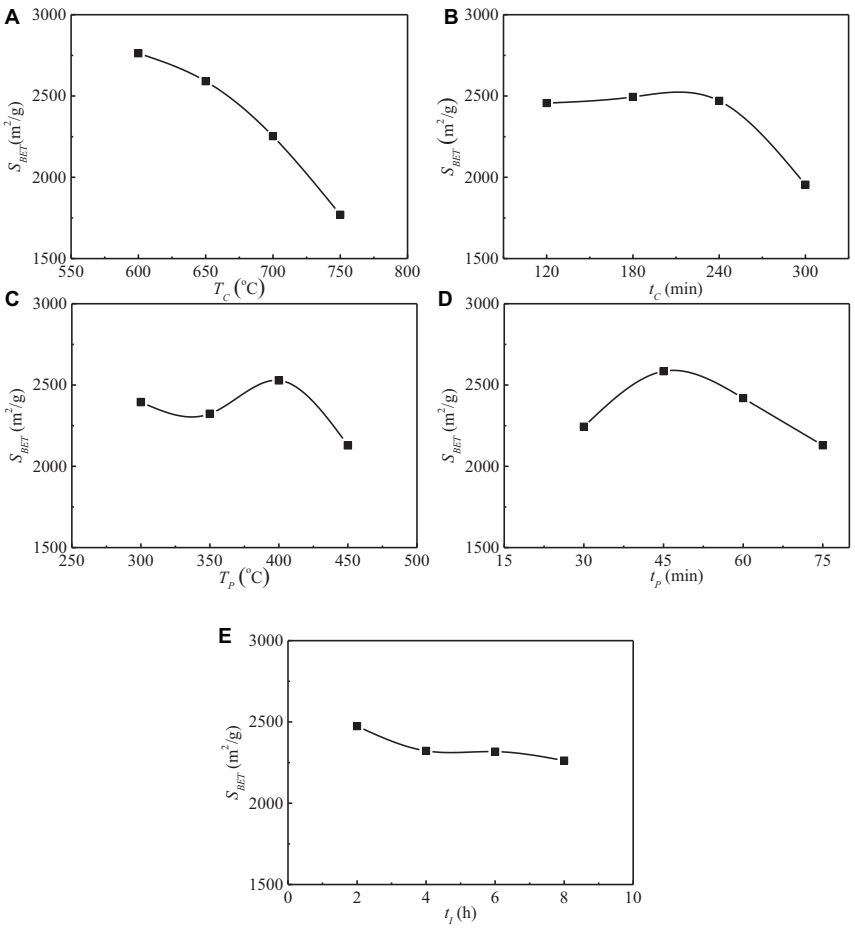

FIGURE 2 | Influences of experimental factors on the specific surface area of SAC. **(A)** Influence of carbonization temperature. **(B)** Influence of carbonization time. **(C)** Influence of pre-activation temperature. **(D)** Influence of pre-activation time. **(E)** Influence of impregnation time.

TABLE 6 | The range analysis of specific pore volume.

	T_C A (°C)	t_C B (min)	T_P C (°C)	t_P D (min)	t_I E (h)	V (cm^3/g)
K_1	9.39	5.82	5.43	5.47	5.95	
K_2	5.80	6.27	5.89	5.97	5.50	
K_3	3.83	5.48	5.85	5.88	5.70	
K_4	3.04	4.49	4.89	4.74	4.91	Σ = 22.06
k_1	2.35	1.46	1.36	1.37	1.49	Σ/16 = 1.38
k_2	1.45	1.57	1.47	1.49	1.38	
k_3	0.96	1.37	1.46	1.47	1.43	
k_4	0.76	1.12	1.22	1.19	1.23	
R	1.59	0.45	0.25	0.30	0.26	

which indicates that the carbonization temperature has the greatest influence on the specific surface area of activated carbon, followed by carbonization time and pre-activation time, while the pre-activation temperature and impregnation time have little effect on the specific surface area. The detailed influence of experimental factors on the specific surface area is shown in **Figure 2**.

The average specific surface area of activated carbon prepared at 600°C reached 2,762.6 m^2/g, and the specific surface area of activated carbon gradually decreased with the increase of carbonization temperature. When the carbonization temperature exceeds 600°C, the continuous increase of temperature will destroy the internal structure of carbon products, thus affecting the formation of initial pores, and ultimately leading to the reduction of specific surface area of activated carbon (Li et al., 2017). When the carbonization time increased from 120 to 240 min, the average specific surface area of activated carbon could hardly observe any change, but when the carbonization time increased from 240 to 300 min, the specific surface area decreased sharply from 2,470.1 to 1,954.8 m^2/g, with a decrease of 20.9%. Therefore, the carbonization time should not be too long for the preparation of activated carbon from sargassum. In the pre-activation stage, the raw materials are activated to a certain extent due to the dehydration reaction between KOH and carbon atoms. In addition, molecular crosslinking and polycondensation reactions take place in the raw materials at this stage, and some tar substances and non-carbon elements such as H and O are discharged (Biloé et al., 2002). When the pre-activation temperature is 400°C, the dehydration reaction of KOH and the dehydration reaction between hydroxyl groups in raw materials have achieved good results. Therefore, the specific surface area of activated carbon prepared at this pre-activation temperature is

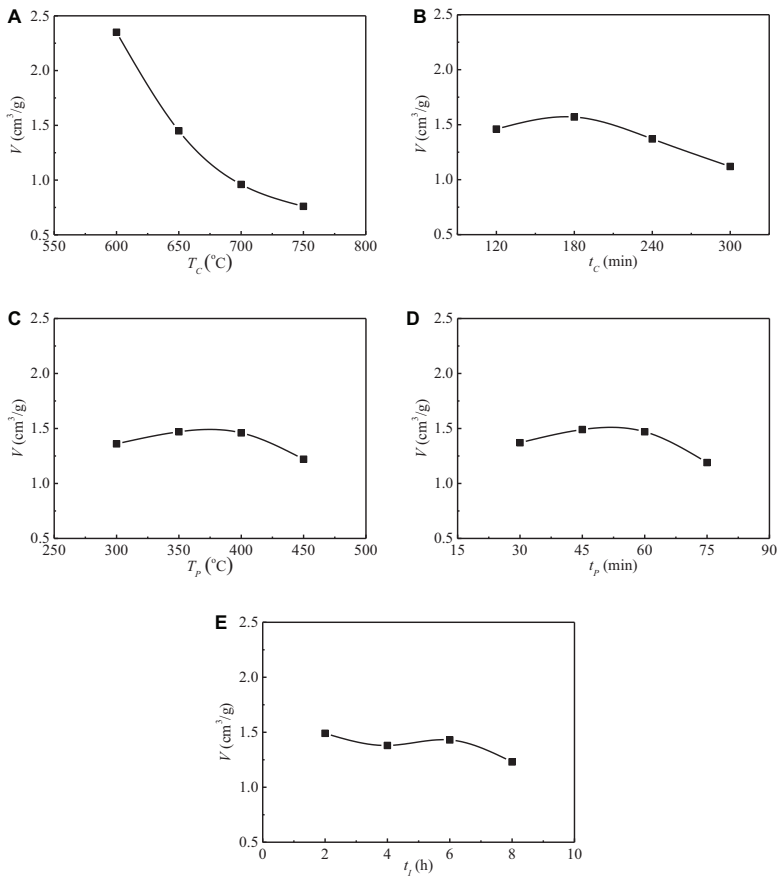

FIGURE 3 | Influences of various factors on the specific pore volume of SAC. **(A)** Influence of carbonization temperature. **(B)** Influence of carbonization time. **(C)** Influence of pre-activation temperature. **(D)** Influence of pre-activation time. **(E)** Influence of impregnation time.

the largest. The specific surface area of activated carbon gradually increased with the increase of pre-activation time until the time increased to 45 min, after which the specific surface area showed a trend of gradual decrease with the continuous increase of pre-activation time. At the beginning of the reaction, more and more carbon atoms are consumed and the initial pore structure is formed with the increase of pre-activation time. However, with the further increase of time, the pore wall of some initial micropores will collapse due to excessive reaction with activator, resulting in the decrease of specific surface area (Li et al., 2017). There is only an insignificant decrease in the specific surface area of activated carbon with the increase of impregnation time. The alkali soluble substances in the raw materials can be removed by potassium hydroxide impregnation, which is conducive to the increase of adsorption sites on the surface of activated carbon, thus increasing the specific surface area of the prepared activated carbon. However, if the impregnation time is too long, cracks and agglomerations will appear on the surface of carbon materials, resulting in the decrease of specific surface area (Muniandy et al., 2014). Especially in the case of high temperature impregnation, the effect of impregnation is stronger, so the impregnation time should not be too long.

Variance Analysis of Specific Surface Area

The variance analysis of specific surface area is shown in **Table 5**.

In the analysis of variance, the effect of impregnation time on the specific surface area and specific pore volume of activated carbon is small enough to be ignored, so the data of impregnation time column can be regarded as a blank column. According to the results of variance analysis, the effect of carbonization temperature on the specific surface area of SAC is very significant, the effect of carbonization time on the specific surface area of SAC is significant, and the effect of pre-activation temperature, pre-activation time and impregnation time on the specific surface area of SAC is not significant. Therefore, the adjustment of carbonization temperature is mainly selected to realize the regulation of specific surface area of SAC, followed by the adjustment of carbonization time. While the pre-activation temperature, pre-activation time and impregnation time can be selected arbitrarily within the range of meeting the experimental requirements.

Effect of Experimental Factors on Specific Pore Volume of SAC

Range Analysis of Specific Pore Volume

The range analysis of specific pore volume is shown in **Table 6**.

It can be seen from **Table 6** that the range of specific pore volume is $R_A > R_B > R_D > R_E > R_C$, which indicates that the carbonization temperature has the greatest influence on the specific pore volume of activated carbon, followed by carbonization time, while the pre-activation time, pre-activation temperature, and impregnation time have little effect on the specific pore volume. The detailed influence of experimental factors on the specific pore volume is shown in **Figure 3**.

As the carbonization temperature increased from 600 to 750°C, the specific pore volume of activated carbon decreased from 2.35 to 0.76 cm^3/g, with a reduction of 67.7%, indicating that carbonization temperature has a significant effect on the specific pore volume of activated carbon. Compared with the carbonization temperature, the effects of carbonization time, pre-activation temperature, pre-activation time, and impregnation time on the specific pore volume of activated carbon are almost negligible.

Variance Analysis of Specific Pore Volume

The variance analysis of specific pore volume is shown in **Table 7**.

TABLE 7 | The variance analysis of specific pore volume.

SV	SS	df	MS	F	Effect
A	6.02	3	2.01	54.40	Very significant
B	0.43	3	0.14	3.87	Not significant
C	0.16	3	0.05	1.47	Not significant
D	0.24	3	0.08	2.13	Not significant
Error	0.15	4	0.04		

$F_{0.01}(3, 4) = 16.69$; $F_{0.05}(3, 4) = 6.59$.

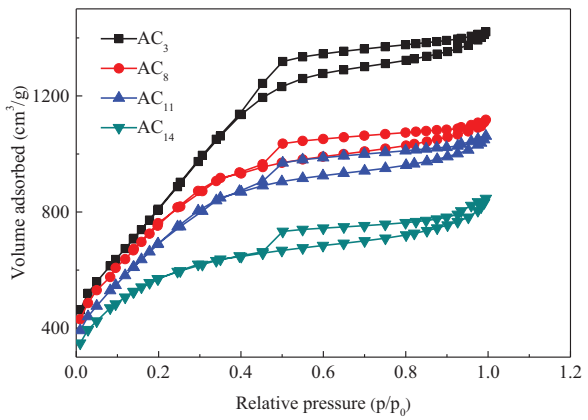

FIGURE 4 | N_2 adsorption-desorption isotherms of SACs.

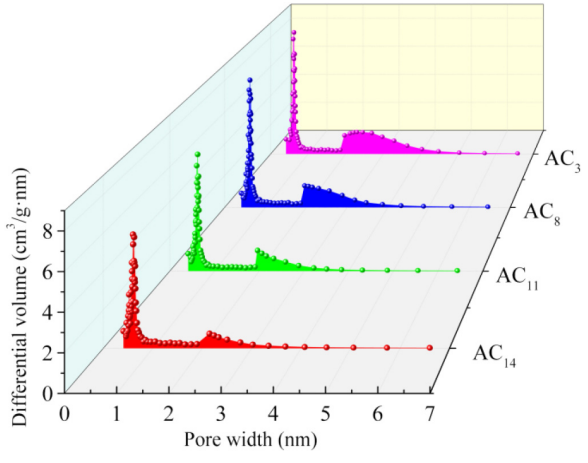

FIGURE 5 | Pore size distribution of prepared activated carbons.

According to the results of variance analysis, the effect of carbonization temperature on the specific pore volume of SAC is very significant, the effect of carbonization time, pre-activation temperature, pre-activation time, and impregnation time on the specific pore volume of SAC is not significant. Therefore, the adjustment of carbonization temperature is mainly selected to realize the regulation of specific pore volume of SAC. While the carbonization time, pre-activation temperature, pre-activation time, and impregnation time can be selected arbitrarily within the range of meeting the experimental requirements.

Material Properties of SACs

Pore Structure Characteristics of SACs

Nitrogen adsorption–desorption isotherms of SACs prepared at different carbonization temperatures are shown in **Figure 4**.

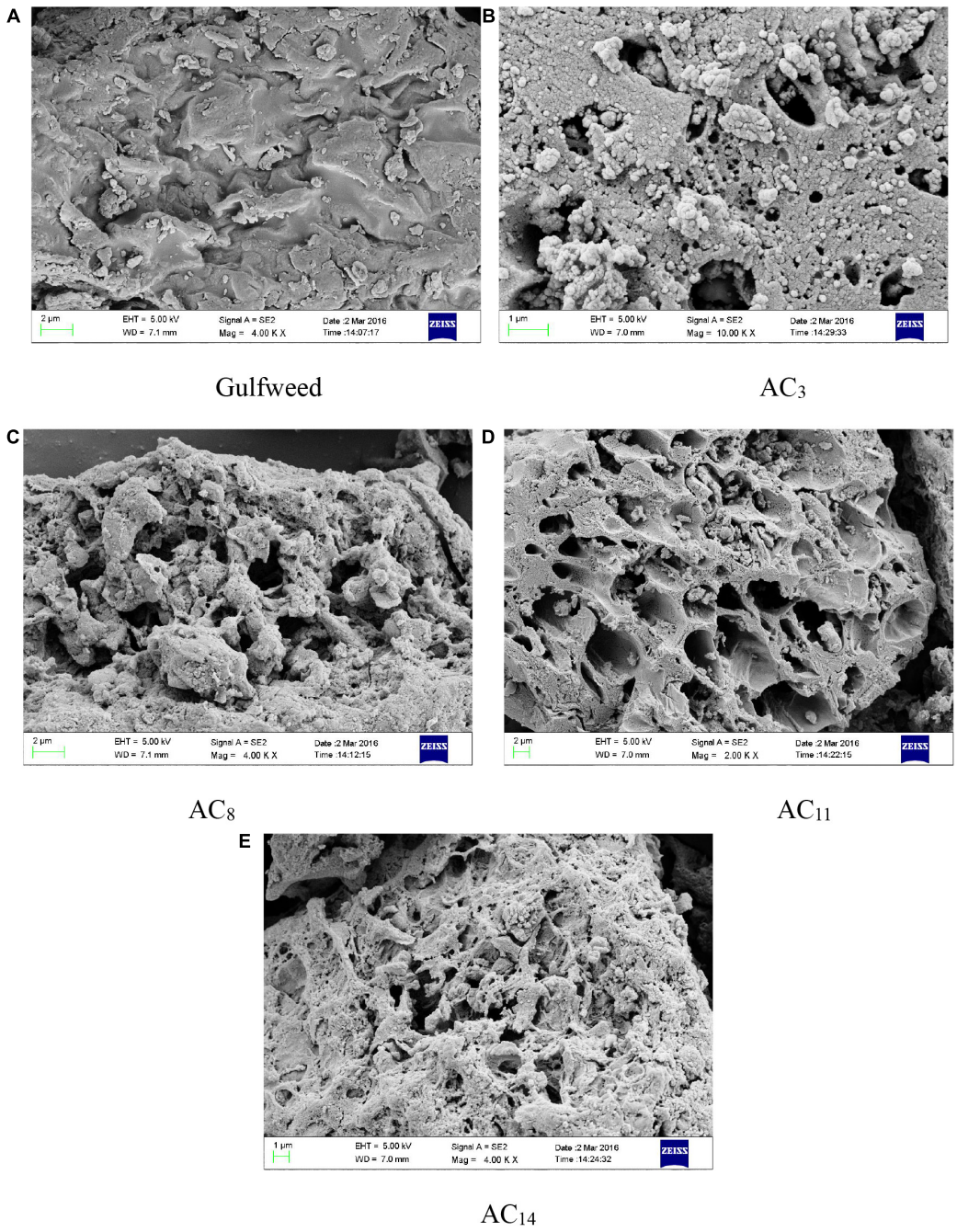

FIGURE 6 | SEM of gulfweed and activated carbons. **(A)** SEM of gulfweed. **(B)** SEM of AC_3. **(C)** SEM of AC_8. **(D)** SEM of AC_{11}. **(E)** SEM of AC_{14}.

As can be seen from **Figure 4**, although the nitrogen adsorption capacity of activated carbon prepared at different carbonization temperatures is different, the adsorption–desorption isotherms of all samples show typical IV curve characteristics. At the low relative pressure stage, the nitrogen adsorption of activated carbon mainly occurs in the micropores. The sharp increase of nitrogen adsorption at this stage indicates that there are a large number of micropores in activated carbon. With the increase of relative pressure, the continuous increase of nitrogen adsorption is observed, instead of the adsorption platform, indicating that there are a certain number of small mesopores in activated carbon. When the relative pressure is 0.5–1, obvious hysteresis loop appeared on all adsorption isotherms, indicating the existence of mesopores or macropores in the prepared activated carbon. The pore size distribution of activated carbons is shown in **Figure 5**.

The pore size distribution of the four groups of activated carbon is relatively concentrated, and the pore diameter is almost all distributed within 6 nm, in which the micropore diameter is mainly concentrated in 0.4–0.8 nm, the mesopore diameter is mainly concentrated in 2–4 nm, and the number of micropores is significantly higher than that of mesopores. The pore structure with a diameter of 0.4–1 nm can provide a large amount of effective internal surface area for the adsorption of electrolyte ions, while the pore structure with a diameter of 2–4 nm can provide a low resistance transport channel for ion transport into the activated carbon (Baughman et al., 2002; Chmiola et al., 2006; Huang et al., 2008; Largeot et al., 2008). According to the N_2 adsorption data, most of the pore sizes of SAC are in the range of 0.4–0.1 nm and 2–4 nm. Therefore, SAC has great

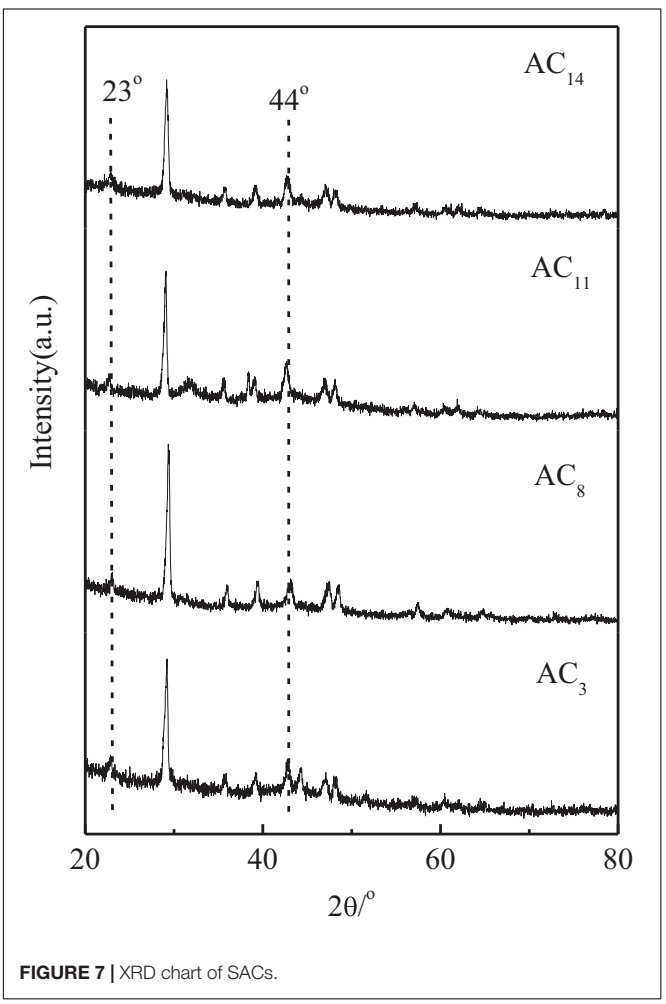

FIGURE 7 | XRD chart of SACs.

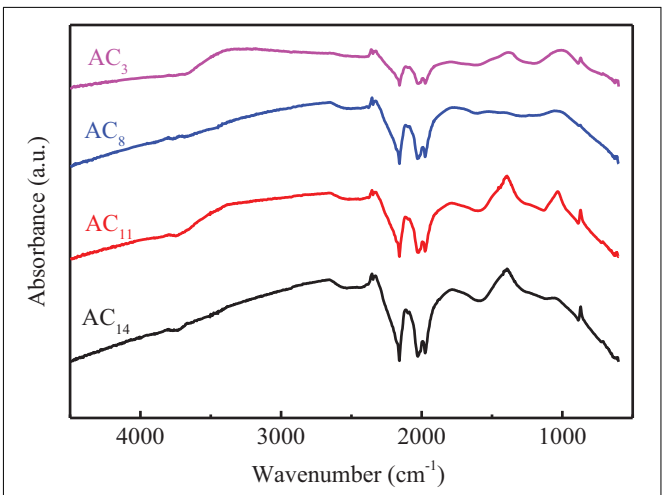

FIGURE 8 | FT-IR spectrum of SACs.

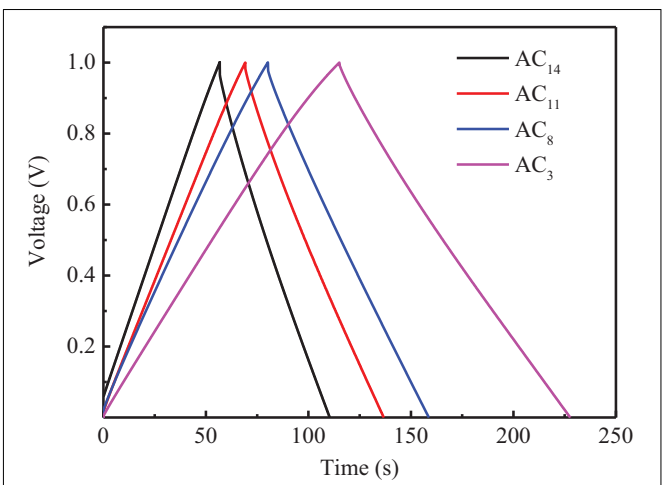

FIGURE 9 | GCD curves of SACs at the current density of 0.5 A/g.

TABLE 8 | Gravimetric capacitance of SACs at different current densities.

Sample	Gravimetric capacitance at different current densities (F/g)					
	0.1 A/g	0.2 A/g	0.5 A/g	1 A/g	2A/g	5 A/g
AC_3	276.6	259.3	241.8	235.7	230.0	221.4
AC_8	251.3	239.2	224.7	217.6	213.5	206.5
AC_{11}	230.0	218.1	206.8	195.6	193.0	184.3
AC_{14}	164.9	154.3	145.1	141.2	139.4	137.8

potential to show good electrochemical performance when used in supercapacitors.

Surface Morphology of SACs

The SEM images of sargassum and SACs prepared at different carbonization temperatures are shown in **Figure 6**. The surface of sargassum raw material is smooth and tight, and almost no pore structure is observed except for some powder debris on the surface, which is caused by the crushing process. The surface of activated carbon after activation treatment is loose and porous, and there are a large number of circular, reticular and fractured pore structures. This is the result of the activation reaction, in which the activator consumes carbon atoms to form a large number of pore structures. In the process of carbonization, the release of tar and volatile matter in biomass raw materials will also lead to the formation of a small amount of initial pore structure, which provides a channel for activator in the impregnation process, so that the activator and the raw material can be mixed better. In addition, potassium vapor is produced in the process of activation at high temperature, and the potassium vapor passes through the pore channel and the carbon layer, forming new pore structure (Gomis-Berenguer et al., 2017).

XRD Analysis of SACs

The XRD patterns of SACs are shown in **Figure 7**. The XRD patterns of SACs demonstrate two sharp diffraction peaks at 2θ = 23°and 44°, which corresponding to (0 0 2) and (1 0 0) diffractions for carbon. This indicates that SACs have a certain graphite microcrystalline structure (Zheng et al., 2012). Activated carbons with huge specific surface area usually have a relatively poor electrical conductivity due to their abundant pore structures, the existence of graphite microcrystalline can greatly improve their electrical conductivity, which resulted for the improvement of their electrochemical performance.

The FT-IR Analysis of SACs

The surface functional groups are associated with the electrochemical performance of the carbon materials by influencing their wettability, polarity and stability (Rychagov et al., 2001; Chen et al., 2003; Fang et al., 2006; Kim et al., 2006; Huang et al., 2007). In addition, the existence of some surface functional groups can improve the capacitance by generating pseudocapacitance (Kim et al., 2002). The FT-IR spectra of SACs are shown in **Figure 8**, the band is observed around the region of 1,050 cm^{-1} which could be attributed to the stretching vibrations of the C–O bonds of esters, alcohols, phenols or ethers (Tongpoothorn et al., 2011). The band at 1,779 cm^{-1}, observed in the spectrum is attributed to the C=O stretching vibration of nonaromatic carboxyl groups with higher intensity in the spectrum resulting from the partial dehydrogenation (Bedin et al., 2016). The presence of the above two surface functional groups contributes to the improvement of the electrochemical performance of activated carbon in alkaline electrolyte. In addition, the bands at 2,661 cm^{-1} in SACs might be ascribed to the traces of potassium carbonates active centres beside metallic potassium that could be produced at 873 K (Gomez-Serrano et al., 1996; Ei-Hendawy, 2006). This indicates that in spite of the extremely prolonged washing, a trace amount of potassium remained chemical bound inside the pore structure.

Electrochemical Properties of SACs

Gravimetric Capacitance of SACs

The GCD curves of the supercapacitors at the current density of 0.5 A/g are shown in **Figure 9**. It can be seen from the figure that all curves show good isosceles triangle shape, indicating that the supercapacitors have good double-layer capacitance properties (Zhou et al., 2014). In addition, there is almost no voltage drop at the moment when the supercapacitors change from charging to discharging, which indicates that SACs have low equivalent series resistance and high charge–discharge efficiency. Electrode materials with larger capacitance and smaller mass have greater potential in some applications, hence, gravimetric capacitance is a very important property for carbon electrode materials (Dong et al., 2012). The gravimetric capacitance of SACs is calculated

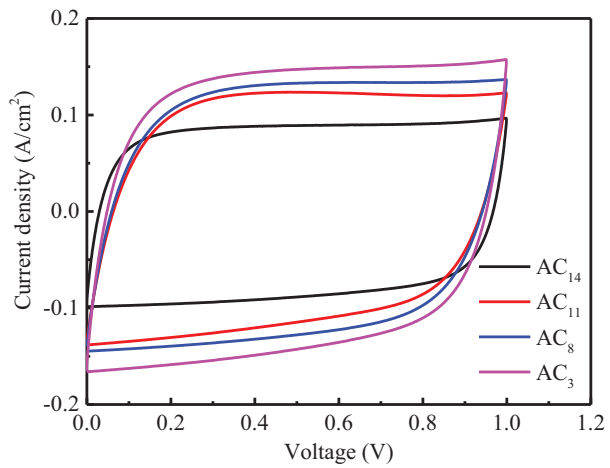

FIGURE 10 | CV curves of SACs at the scan rate of 200 mV/s.

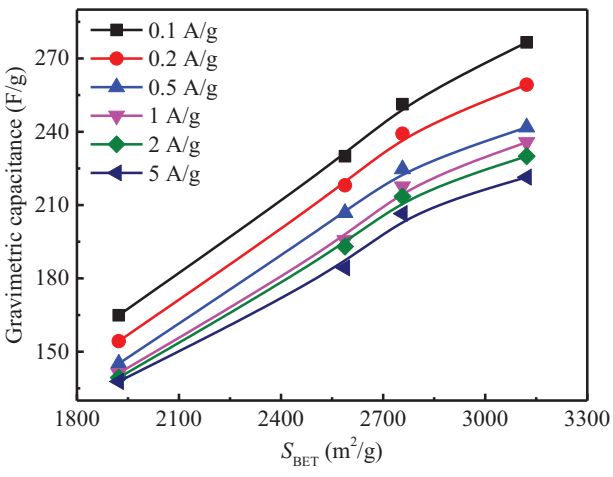

FIGURE 11 | Relationship between gravimetric capacitance and S_{BET} of SACs.

according to the GCD curves of the supercapacitors, and the capacitance values are shown in **Table 8**.

Cyclic Voltammetry Characteristics of SACs

It can be observed from **Figure 10** that the CV curves of SACs show excellent rectangular shapes from 0 to 1 V, indicating an ideal electrical double layer effect of the tested supercapacitors. Moreover, inexistence of any redox peaks at CV curves is observed, implying the absence of pseudocapacitance. Even the supercapacitors are measured at a relatively high scan rate of 200 mV/s, the CV curves still show better rectangular shapes, indicating that the SAC electrodes possess relatively smaller equivalent series resistance and strong ion transport ability, which leads to the quick charge propagation in carbon electrodes.

Relationship Between Gravimetric Capacitance and Specific Surface Area of SACs

The gravimetric capacitance of activated carbon is directly proportional to the specific surface area according to the electric double layer theory, but in fact, the gravimetric capacitance of activated carbon is affected by many factors, such as pore size distribution, surface functional groups, graphitization degree, etc. In order to improve the gravimetric capacitance of SAC by adjusting its pore structure, the relationship between gravimetric capacitance and specific surface area was studied, the results are shown in **Figure 11**. It can be seen from the figure that the gravimetric capacitance and specific surface area of SAC present a good linear relationship at all current densities. This is due to the similar material properties and pore size distributions of AC_3, AC_8, AC_{11}, and AC_{14}, with the increase of specific surface area, the effective adsorption surface area and ion transport channel of activated carbon increase linearly, resulting in more electric double-layer capacitance.

CONCLUSION

The most effective measure to regulate the specific surface area of SAC is to adjust the carbonization temperature, followed by the adjustment of carbonization time. With the increase of carbonization temperature, the specific surface area of SAC continued to decrease to a large extent. With the increase of carbonization time, the specific surface area of SAC first increased and then decreased. The effects of pre-activation temperature, pre-activation time and impregnation time on the specific surface area of SAC are not significant. The most effective measure to regulate the specific pore volume of SAC is to adjust the carbonization temperature. With the increase of carbonization temperature, the specific pore volume of SAC decreases gradually. The effects of carbonization time, pre-activation temperature, pre-activation time and impregnation time on the specific pore volume of SAC are not significant. All SACs have developed pore structure and large specific surface area, and exhibits good electrochemical performance. All the activated carbons prepared in this study have similar material properties and pore size distribution, on this basis, the gravimetric capacitance and specific surface area show a good linear relationship.

DATA AVAILABILITY STATEMENT

The original contributions presented in the study are included in the article/supplementary material, further inquiries can be directed to the corresponding author.

AUTHOR CONTRIBUTIONS

SL mainly contributed to the experimental design and article writing. TX mainly contributed to provide useful suggestions for the experiment. YW and PL mainly contributed to the experimental operation. WK and SL mainly contributed to the test characterization of material properties. XS and XW mainly contributed to the data analysis of the experimental results. All authors contributed to the article and approved the submitted version.

FUNDING

This study was supported by the Doctoral Fund of Shandong Jianzhu University (XNBS1838) and Shandong Provincial Natural Science Foundation (ZR2019BEE059).

ACKNOWLEDGMENTS

We are grateful to the Shandong University for providing equipment support.

REFERENCES

Abioye, A. M., and Ani, F. N. (2015). Recent development in the production of activated carbon electrodes from agricultural waste biomass for supercapacitors: a review. *Renew. Sust. Energ. Rev.* 52, 1282–1293. doi: 10.1016/j.rser.2015.07.129

Baughman, R. H., Zakhidov, A. A., and Heer, W. A. D. (2002). Carbon nanotubes–. *Science* 297, 787–793.

Bedin, K. C., Martins, A. C., Cazetta, A. L., Pezoti, O., and Almeida, V. C. (2016). KOH-activated carbon prepared from sucrose spherical carbon: adsorption equilibrium, kinetic and thermodynamic studies for methylene blue removal. *Chem. Eng. J.* 286, 476–484. doi: 10.1016/j.cej.2015.10.099

Biloé, S., Goetz, V., and Guillot, A. (2002). Optimal design of an activated carbon for an adsorbed natural gas storage system. *Carbon* 40, 1295–1308. doi: 10.1016/s0008-6223(01)00287-1

Cao, H., Zhou, X., Deng, W., Ma, Z., Liu, Y., and Liu, Z. (2018). Layer structured graphene/porous $ZnCo_2O_4$ composite film for high performance flexible lithium-ion batteries. *Chem. Eng. J.* 343, 654–661. doi: 10.1016/j.cej.2018.03.001

Cao, Y., Wang, X., Gu, Z., Fan, Q., Gibbons, W., Gadhamshetty, V., et al. (2018). Potassium chloride templated carbon preparation for supercapacitor. *J. Power Sources* 384, 360–366. doi: 10.1016/j.jpowsour.2018.02.079

Chen, H., Guo, Y. C., Wang, F., Wang, G., Qi, P. R., Guo, X. H., et al. (2017). An activated carbon derived from tobacco waste for use as a supercapacitor electrode material. *New Carbon Mater.* 32, 592–599. doi: 10.1016/s1872-5805(17)60140-9

Chen, W. C., Wen, T. C., and Teng, H. (2003). Polyaniline–deposited porous carbon electrode for supercapacitor. *Electrochim. Acta* 48, 641–649. doi: 10.1016/s0013-4686(02)00734-x

Chmiola, J., Yushin, G., Dash, R., and Gogotsi, Y. (2006). Effect of pore size and surface area of carbide derived carbons on specific capacitance. *J. Power Sources* 158, 765–772. doi: 10.1016/j.jpowsour.2005.09.008

Deng, J., Li, M., and Wang, Y. (2016). Biomass-derived carbon: synthesis and applications in energy storage and conversion. *Green Chem.* 18, 4824–4854. doi: 10.1039/c6gc01172a

Dong, X. C., Wang, X. W., Wang, L., Song, H., Li, X. G., Wang, L. H., et al. (2012). Synthesis of a MnO_2-graphene foam hybrid with controlled MnO_2 particle shape and its use as a supercapacitor electrode. *Carbon* 50, 4865–4870. doi: 10.1016/j.carbon.2012.06.014

Ei-Hendawy, A. N. A. (2006). Variation in the FTIR spectra of a biomass under impregnation, carbonization and oxidation conditions. *J Anal Appl Pyrolysis* 75, 159–166. doi: 10.1016/j.jaap.2005.05.004

Fang, B., Wei, Y. Z., and Kumagai, M. (2006). Modified carbon materials for high–rate EDLCs application. *J. Power Sources* 155, 487–491. doi: 10.1016/j.jpowsour.2005.04.012

Farma, R., Deraman, M., Awitdrus, A., Talib, I. A., Taer, E., Basri, N. H., et al. (2013). Preparation of highly porous binderless activated carbon electrodes from fibres of oil palm empty fruit bunches for application in supercapacitors. *Bioresour. Technol.* 132, 254–261. doi: 10.1016/j.biortech.2013.01.044

Gomez-Serrano, V., Pastor-Villegas, J., Perez-Florindo, A., Duran-Valle, A. C., and Valenzuela-Calahorro, C. (1996). FT-IR study of rockrose and char and activated carbon. *J. Anal. Appl. Pyrolysis* 36, 71–80. doi: 10.1016/0165-2370(95)00921-3

Gomis-Berenguer, A., Velasco, L. F., Velo-Gala, I., and Ania, C. O. (2017). Photochemistry of nanoporous carbons: perspectives in energy conversion and environmental remediation. *J. Colloid Interface Sci.* 490, 879–901. doi: 10.1016/j.jcis.2016.11.046

Guo, D., Song, X., Tan, L., Ma, H., Pang, H., Wang, X., et al. (2018a). Metal-organic framework template-directed fabrication of well-aligned pentagon-like hollow transition-metal sulfides as the anode and cathode for high-performance asymmetric supercapacitors. *ACS Appl. Mater. Interfaces* 10, 42621–42629. doi: 10.1021/acsami.8b14839

Guo, D., Zhang, L., Song, X. M., Tan, L. C., Ma, H. Y., Jiao, J., et al. (2018b). $NiCo_2O_4$ nanosheets grown on interconnected honeycomb-like porous biomass carbon for high performance asymmetric supercapacitors. *New J. Chem.* 42, 8478–8484. doi: 10.1039/c8nj00515j

Guo, D., Song, X., Tan, L., Ma, H., Sun, W., Pang, H., et al. (2019). A facile dissolved and reassembled strategy towards sandwich-like rGO@NiCoAl-LDHs with excellent supercapacitor performance. *Chem. Eng. J.* 356, 955–963. doi: 10.1016/j.cej.2018.09.101

Hao, L., Li, X. L., and Zhi, L. J. (2013). Carbonaceous electrode materials for supercapacitors. *Adv. Mater.* 25, 3899–3904. doi: 10.1002/adma.201301204

Hou, Y., Chai, D., Li, B., Pang, H., Ma, H., Wang, X., et al. (2019). Polyoxometalate-incorporated metallacalixarene@graphene composite electrodes for high-performance supercapacitors. *ACS Appl. Mater. Interfaces* 11, 20845–20853. doi: 10.1021/acsami.9b04649

Huang, J. S., Sumpter, B. G., and Meunier, V. (2008). A universal model for nanoporous carbon supercapacitors applicable to diverse pore regimes, carbon materials, and electrolytes. *Chem. Eur. J.* 14, 6614–6626. doi: 10.1002/chem.200800639

Huang, Q. H., Wang, X. Y., Li, J., Dai, C. L., Gamboa, S., and Sebastian, P. J. (2007). Nickel hydroxide/activated carbon composite electrodes for electrochemical capacitors. *J. Power Sources* 164, 425–429. doi: 10.1016/j.jpowsour.2006.09.066

Kim, C. H., Pyun, S. I., and Shin, H. C. (2002). Kinetics of double–layer charging/discharging of activated carbon electrodes: role of surface acidic functional groups. *Electrochem. Soc.* 149, 93–98.

Kim, I. H., Kim, J. H., Cho, B. W., and Kim, K. B. (2006). Synthesis and electrochemical characterization of vanadium oxide on carbon nanotube film substrate for pseudocapacitor applications. *J. Electrochem. Soc.* 153, 1451–1458.

Largeot, C., Portet, C., Chmiola, J., Taberna, P. L., Gogotsi, Y., and Simon, P. (2008). Relation between the ion size and pore size for an electric double–layer capacitor. *J. Am. Chem. Soc.* 130, 2730–2731. doi: 10.1021/ja7106178

Lee, K. S., Park, M. S., and Kim, J. D. (2017). Nitrogen doped activated carbon with nickel oxide for high specific capacitance as supercapacitor electrodes. *Colloids Surf.A* 533, 323–329. doi: 10.1016/j.colsurfa.2017.09.008

Li, S. J., Han, K. H., Gao, Y., Zhang, M. Y., Wang, Q., and Zhang, L. H. (2019). Synergistic optimization of double layer capacitance and pseudocapacitance of activated carbon by nickel oxide loading. *Int. J. Electrochem. Sci.* 14, 10775–10789. doi: 10.20964/2019.12.53

Li, S. J., Han, K. H., Li, J. X., Li, M., and Lu, C. M. (2017). Preparation and characterization of super activated carbon produced from gulfweed by KOH activation. *Microporous Mesoporous Mater.* 243, 291–300. doi: 10.1016/j.micromeso.2017.02.052

Li, W., Tan, S., Shi, Y., and Li, S. J. (2015). Utilization of *Sargassum* based activated carbon as a potential waste derived catalyst for low temperature selective catalytic reduction of nitric oxides. *Fuel* 160, 35–42. doi: 10.1016/j.fuel.2015.07.045

Liu, C., Ren, Q. Q., Zhang, S. W., Yin, B. S., Que, L. F., Zhao, L., et al. (2019). High energy and power lithium-ion capacitors based on Mn_3O_4/3D-graphene as anode and activated polyaniline-derived carbon nanorods as cathode. *Chem. Eng. J.* 370, 1485–1492. doi: 10.1016/j.cej.2019.04.044

Liu, M. X., Gan, L. H., Xiong, W., Zhu, D. Z., Xu, Z. J., and Chen, L. W. (2013). Partially graphitic micro– and mesoporous carbon microspheres for supercapacitors. *Chin. Chem. Lett.* 24, 1037–1040. doi: 10.1016/j.cclet.2013.07.013

Miller, E. E., Hua, Y., and Tezel, F. H. (2018). Materials for energy storage: review of electrode materials and methods of increasing capacitance for supercapacitors. *J. Energy Storage* 20, 30–40. doi: 10.1016/j.est.2018.08.009

Muniandy, L., Adam, F., Mohamed, A. R., and Ng, E. P. (2014). The synthesis and characterization of high purity mixed microporous/mesoporous activated carbon from rice husk using chemical activation with NaOH and KOH. *Microporous Mesoporous Mater.* 197, 316–323. doi: 10.1016/j.micromeso.2014.06.020

Pintor, M. J., Jean-Marius, C., Jeanne-Rose, V., Taberna, P. L., Simon, P., Gamby, J., et al. (2013). Preparation of activated carbon from Turbinaria turbinata seaweeds and its use as supercapacitor electrode materials. *Comptes Rendus Chim.* 16, 73–79. doi: 10.1016/j.crci.2012.12.016

Qiu, W., Xiao, H., Yu, M., Li, Y., and Lu, X. (2018). Surface modulation of $NiCo_2O_4$ nanowire arrays with significantly enhanced reactivity for ultrahigh-energy supercapacitors. *Chem. Eng. J.* 352, 996–1003. doi: 10.1016/j.cej.2018.04.118

Rychagov, A. Y., Urisson, N. A., and Vol'Fkovich, Y. M. (2001). Electrochemical characteristics and properties of the surface of activated carbon electrodes in a double–layer capacitor. *Russ. J. Electrochem.* 37, 1172–1179.

Saeed, G., Kumar, S., Kim, N. H., and Lee, J. H. (2018). Fabrication of 3D graphene-CNTs/α -MoO_3 hybrid film as an advance electrode material for asymmetric supercapacitor with excellent energy density and cycling life. *Chem. Eng. J.* 352, 268–276. doi: 10.1016/j.cej.2018.07.026

Shao, J., Ma, F., Wu, G., Dai, C., Geng, W., Song, S., et al. (2017). In-situ MgO ($CaCO_3$) templating coupled with KOH activation strategy for high yield preparation of various porous carbons as supercapacitor electrode materials. *Chem. Eng. J.* 321, 301–313. doi: 10.1016/j.cej.2017.03.092

Shao, J., Song, M., Wu, G., Zhou, Y., Wan, J., Ren, X., et al. (2018). 3D carbon nanocage networks with multiscale pores for high-rate supercapacitors by flower-like template and in-situ coating. *Energy Stor. Mater.* 13, 57–65. doi: 10.1016/j.ensm.2017.12.023

Simon, P., and Gogotsi, Y. (2008). Materials for electrochemical capacitors. *Nat. Mater.* 7, 845–854.

Titirici, M. M., and Antonietti, M. (2010). Chemistry and materials options of sustainable carbon materials made by hydrothermal carbonization. *Chem. Soc. Rev.* 39, 103–116. doi: 10.1039/b819318p

Tongpoothorn, W., Sriuttha, M., Homchan, P., Chanthai, S., and Ruangviriyachai, C. (2011). Preparation of activated carbon derived from *Jatropha curcas* fruit shell by simple thermo-chemical activation and characterization of their physico-chemical properties. *Chem. Eng. Res. Des.* 89, 335–340. doi: 10.1016/j.cherd.2010.06.012

Tseng, L.-H., Hsiao, C.-H., Nguyen, D. D., Hsieh, P.-Y., Lee, C.-Y., and Tai, N.-H. (2018). Activated carbon sandwiched manganese dioxide/graphene ternary composites for supercapacitor electrodes. *Electrochim. Acta* 266, 284–292. doi: 10.1016/j.electacta.2018.02.029

Wang, D., Wang, K., Sun, L., Wu, H., Wang, J., Zhao, Y., et al. (2018). MnO_2 nanoparticles anchored on carbon nanotubes with hybrid supercapacitor-battery behavior for ultrafast lithium storage. *Carbon* 139, 145–155. doi: 10.1016/j.carbon.2018.06.046

Wang, D., Xu, Z., Lian, Y., Ban, C., and Zhang, H. (2019). Nitrogen self-doped porous carbon with layered structure derived from porcine bladders for high-performance supercapacitors. *J. Colloid Interface Sci.* 542, 400–409. doi: 10.1016/j.jcis.2019.02.024

Wang, D. B., Geng, Z., Li, B., and Zhang, C. M. (2015). High performance electrode materials for electric double–layer capacitors based on biomass–derived activated carbons. *Electrochim. Acta* 173, 377–384. doi: 10.1016/j.electacta.2015.05.080

Wang, J. C., and Kaskel, S. (2012). KOH activation of carbon–based materials for energy storage. *J. Mater. Chem. A* 22, 23710–23725. doi: 10.1039/c2jm34066f

Wang, J.-G., Liu, H., Zhang, X., Shao, M., and Wei, B. (2018). Elaborate construction of N/S-co-doped carbon nanobowls for ultrahigh-power supercapacitors. *J. Mater. Chem. A* 6, 17653–17661. doi: 10.1039/c8ta07573e

White, R. J., Budarin, V., Luque, R., Clark, J. H., and Macquarrie, D. J. (2009). Tuneable porous carbonaceous materials from renewable resources. *Chem. Soc. Rev.* 38, 3401–3418. doi: 10.1039/b822668g

Xiao, Y., Long, C., Zheng, M. T., Dong, H. W., Lei, B. F., Zhang, H. R., et al. (2014). High-capacity porous carbons prepared by KOH activation of activated carbon for supercapacitors. *Chin. Chem. Lett.* 25, 865–868. doi: 10.1016/j.cclet.2014.05.004

Yu, Y., Wang, C. H., Guo, X., and Chen, J. P. (2015). Modification of carbon derived from *Sargassum* sp. by lanthanum for enhanced adsorption of fluoride. *J. Colloid Interface Sci.* 441, 113–120. doi: 10.1016/j.jcis.2014.10.039

Zhang, J., Xue, J., Li, P., Huang, S., Feng, H., and Luo, H. (2018). Preparation of metal-organic framework-derived porous carbon and study of its supercapacitive performance. *Electrochim. Acta* 284, 328–335. doi: 10.1016/j.electacta.2018.07.102

Zhang, K. J., Liu, M. R., Zhang, T. Z., Min, X. Y., Wang, Z. R., Chai, L. Y., et al. (2019). High-performance supercapacitor energy storage using a carbon material derived from lignin by bacterial activation before carbonization. *J. Mater. Chem. A* 7, 26838–26848. doi: 10.1039/c9ta04369a

Zhang, T., Zheng, M. B., Li, N. W., Lu, H. L., Zhang, S. T., and Cao, J. M. (2013). Macro–microporous carbon for supercapacitors derived from rape seed shell. *Mater. Lett.* 105, 43–46. doi: 10.1016/j.matlet.2013.04.055

Zheng, H. J., Yu, A. M., and Ma, C. A. (2012). Effect of pore characteristics on electrochemical capacitance of activated carbons. *Russ. J. Electrochem.* 48, 1179–1186. doi: 10.1134/s102319351205014x

Zhou, H., Lv, B. L., Xu, Y., and Wu, D. (2014). Synthesis and electrochemical properties of NiO nanospindles. *Mater. Res. Bull.* 50, 399–404. doi: 10.1016/j.materresbull.2013.11.004

Conflict of Interest: SL and TX was employed by company Shandong Energy Group Co., Ltd.

The remaining authors declare that the research was conducted in the absence of any commercial or financial relationships that could be construed as a potential conflict of interest.

Copyright © 2021 Li, Xing, Wang, Lu, Kong, Li, Su and Wei. This is an open-access article distributed under the terms of the Creative Commons Attribution License (CC BY). The use, distribution or reproduction in other forums is permitted, provided the original author(s) and the copyright owner(s) are credited and that the original publication in this journal is cited, in accordance with accepted academic practice. No use, distribution or reproduction is permitted which does not comply with these terms.